Inorg. Chem. **2007**, *46*, 11063–11074

New Potassium Bismuth Thiophosphates Including the Modulated $K_{1.5}Bi_{2.5}(PS_4)_3$

Matthew A. Gave,[†] David P. Weliky,[†] and Mercouri G. Kanatzidis*[,†,‡]

Department of Chemistry, Michigan State University, East Lansing, Michigan 48824, and Department of Chemistry, Northwestern University, Evanston, Illinois, 60208

Received June 20, 2007

The compounds $K_3Bi_3(PS_4)_4$ (**I**), $K_{1.5}Bi_{2.5}(PS_4)_3$ (**II**), and $K_9Bi(PS_4)_4$ (**III**) were synthesized, and their properties are described. Red needles of **I** crystallize in the tetragonal spacegroup *P*4/*ncc* with $a = 21.0116(8)$ Å and $c = 13.3454(10)$ Å and have a three-dimensional Bi/P/S framework structure with large channels occupied by K^+ ions. Deep-red plates of **II** crystallize in the monoclinic super spacegroup $P2/c(\alpha^1/_2\gamma)00$ with $a = 21.8034(12)$ Å, $b = 8.8064(7)$ Å, $c = 10.0333(6)$ Å, and $\beta = 90.004(5)°$. This compound has an incommensurately modulated superstructure with the modulation vector $\mathbf{q} = 0.25\mathbf{a^*} + 0.5\mathbf{b^*} + 0.16\mathbf{c^*}$. Bright-red irregularly shaped blocks of **III** crystallize in the orthorhombic space group $P2_12_12$ with $a = 18.306(4)$ Å, $b = 8.926(2)$ Å, and $c = 9.710(2)$ Å and have a discrete molecular salt structure with mononuclear $[Bi(PS_4)_4]^{9-}$ complexes. The structures reveal that as the relative amount of K_3PS_4 increases, there is a marked decrease in dimensionality of the framework. It was also possible to form a glass with the same stoichiometry as that of compound **I**. When annealed at 320 °C, the glass crystallized into compound **II**. The ^{31}P solid-state NMR spectra are reported, and they are consistent with the crystallographic results.

Introduction

Chalcophosphate compounds generally are semiconductors with medium to wide energy gaps and can exhibit fascinating physical properties including pronounced photoconductivity,[1] photorefractive gain,[2,3] ferroelectricity,[4−6] and electro-optic[7] and second harmonic generation[8] properties. The chalcophosphate anions are a special class of polyanions with broad reactivity and structural characteristics with general formula of $[P_xQ_y]^{z-}$ (Q = S, Se). They can be stabilized as alkali-metal salts[9,10] or coordinating ligands to a variety of metal centers.[11−18] The chemistry of these materials has been substantially developed in the past decade due to the application of the flux synthesis technique, which serves as a medium for the reaction chemistry and a tool for discovery. Bismuth chalcogenide compounds have a great deal of structural diversity due in part to the so-called inert "lone-pair" effect[19−25] and the flexibility in the coordination environment including trigonal-pyramidal,[26] square-pyramidal,[27] and capped-trigonal-prismatic geometries.[28,29] Bismuth can bind to vari-

* To whom correspondence should be addressed. E-mail: m-kanatzidis@northwestern.edu.
[†] Michigan State University.
[‡] Northwestern University.

(1) Galdamez, A.; Manriquez, V.; Kasaneva, J.; Avila, R. E. *Mater. Res. Bull.* **2003**, *38*, 1063−1072.
(2) Odoulov, S. G.; Shumelyuk, A. N.; Brost, G. A.; Magde, K. M. *Appl. Phys. Lett.* **1996**, *69*, 3665−3667.
(3) Shumelyuk, A.; Hryhorashchuk, A.; Odoulov, S. *Phys. Rev. A: At., Mol., Opt. Phys.* **2005**, *72*, 6.
(4) Bourdon, X.; Maisonneuve, V.; Cajipe, V. B.; Payen, C.; Fischer, J. E. *J. Alloys Compd.* **1999**, *283*, 122−127.
(5) Carpentier, C. D.; Nitsche, R. *Mater. Res. Bull.* **1974**, *9*, 1097−1100.
(6) Rogach, E. D.; Sviridov, E. V.; Arnautova, E. A.; Savchenko, E. A.; Protsenko, N. P. *Zh. Tekh. Fiz.* **1991**, *61*, 201−204.
(7) Kroupa, J.; Tyagur, Y. I.; Grabar, A. A.; Vysochanskii, Y. M. *Ferroelectrics* **1999**, *223*, 421−428.
(8) Misuryaev, T. V.; Murzina, T. V.; Aktsipetrov, O. A.; Sherstyuk, N. E.; Cajipe, V. B.; Bourdon, X. *Solid State Commun.* **2000**, *115*, 605−608.
(9) Knaust, J. M.; Dorhout, P. K. *J. Chem. Crystallogr.* **2006**, *36*, 217−223.
(10) Chung, I.; Do, J.; Canlas, C. G.; Weliky, D. P.; Kanatzidis, M. G. *Inorg. Chem.* **2004**, *43*, 2762−2764.
(11) Kanatzidis, M. G. *Curr. Opin. Solid State Mater. Sci.* **1997**, *2*, 139−149.
(12) Coste, S.; Hanko, J.; Bujoli-Doeuff, M.; Louarn, G.; Evain, M.; Brec, R.; Alonso, B.; Jobic, S.; Kanatzidis, M. G. *J. Solid State Chem.* **2003**, *175*, 133−145.
(13) Manriquez, V.; Galdamez, A.; Ruiz-Leon, D. *Mater. Res. Bull.* **2006**, *41*, 1337−1344.
(14) Belkyal, I.; El Azhari, M.; Wu, Y. D.; Bensch, W.; Hesse, K. F.; Depmeier, W. *Solid State Sci.* **2006**, *8*, 59−63.
(15) Gieck, C.; Tremel, W. *Chem.−Eur. J.* **2002**, *8*, 2980−2987.
(16) Coste, S.; Kopnin, E.; Evain, M.; Jobic, S.; Brec, R.; Chondroudis, K.; Kanatzidis, M. G. *Solid State Sci.* **2002**, *4*, 709−716.
(17) Hess, R. F.; Gordon, P. L.; Tait, C. D.; Abney, K. D.; Dorhout, P. K. *J. Am. Chem. Soc.* **2002**, *124*, 1327−1333.
(18) Coste, S.; Kopnin, E.; Evain, M.; Jobic, S.; Payen, C.; Brec, R. *J. Solid State Chem.* **2001**, *162*, 195−203.

10.1021/ic701211a CCC: $37.00
Published on Web 11/20/2007

ous chalcophosphate ligands, as for example in the compounds $KBiP_2S_7$,[26,30] $KBiP_2S_6$,[31] and $K_3Bi(PS_4)_2$,[30] which contain the $[P_2S_7]^{4-}$, $[P_2S_6]^{4-}$, and $[PS_4]^{3-}$ anions, respectively. Each anion can be selectively formed by slightly varying the reaction conditions, and a variety of phases can therefore be rationally synthesized.[32]

The K/Bi/P/S chemistry was further investigated to search for K^+ analogues of the recently reported Tl/Bi/P/S compounds.[33] Due to their monovalency and similar ionic radii, K^+ and Tl^+ are often considered to have similar chemical reactivity and form structurally related compounds. Additionally, related A/M/P/Q (A = K, Rb, Cs; M = Bi, Pb; Q = S, Se) compounds exhibit a reduction in structural dimensionality as the proportion of alkali metal is increased.[31,34−36] Low-dimensional materials are of interest because they may have accessible networks suitable for ion-exchange reactions which can either produce metastable isomorphic analogues, or following structural rearrangement, new compounds.[37] We describe here the compounds $K_3Bi_3(PS_4)_4$ (**I**), $K_{1.5}Bi_{2.5}(PS_4)_3$ (**II**), and $K_9Bi(PS_4)_4$ (**III**). The first two feature unique extended Bi/P/S arrangements with **II** exhibiting an incommensurate superstructure arising from a modulation of the occupation of the Bi/Tl site. The third compound **III** is a molecular salt with an eight-coordinate mononuclear $[Bi(PS_4)_4]^{9-}$ complex.

Experimental Section

Reagents. Chemicals were used as obtained unless otherwise noted: bismuth chunks (Tellurex, Inc., Traverse City, MI, 99.999%), phosphorus (MCB Reagents, Gibbstown, NJ, amorphous red), sublimed sulfur flowers (CCI, Vernon, CA), potassium metal, (Aldrich Chemical Co., Inc., St. Louis, MO). Bismuth was ground in an agate mortar and pestle to ca. 100 mesh. Phosphorus was freeze-dried, and K_2S was prepared by a modified literature preparation.[23,38]

Synthesis. Manipulations of Bi, P, and S were carried out in ambient conditions and then transferred into a Vacuum Atmospheres Dri-Lab glovebox filled with N_2 where the appropriate amount of K_2S was added.

$K_3Bi_3(PS_4)_4$ (I). A mixture of K_2S (0.174 g, 1.6 mmol), Bi (0.3941 1.9 mmol), P (0.0781 g, 2.5 mmol), and S (0.3533 g, 11.0 mmol) was loaded into a fused silica ampule and flame-sealed under a reduced atmosphere of ca. 10^{-4} mbar. After shaking to increase homogeneity, the tube was inserted into a protective ceramic sheath and placed in a furnace. The mixture was heated to 600 °C over 12 h, held there for 12 h, and then cooled back to room temperature over a period of 6 h. An inhomogenous red crystalline ingot that was a mixture of $K_3Bi_3(PS_4)_4$ (**I**) (∼70%), $K_{1.5}Bi_{2.5}(PS_4)_3$ (**II**) (∼20%), $K_3Bi(PS_4)$ (5%), and Bi_2S_3 (∼5%) was isolated. Microprobe analysis averaged over several sample areas of the single crystal used for the diffraction experiments gave an average composition of $K_{1.0}Bi_{1.0}P_{1.4}S_{5.8}$.

$K_{1.5}Bi_{2.5}(PS_4)_3$ (II). An ampule containing a mixture of K_2S (0.039 g, 0.35 mmol), Bi (0.2461 g, 1.2 mmol), P (0.0435 g, 1.4 mmol), and S (0.1709 g, 5.4 mmol) was allowed to react under the same conditions used to produce compound **I**. A homogeneous red crystalline ingot that was composed of air-stable red plates of $K_{1.5}Bi_{2.5}(PS_4)_3$ was isolated in quantitative yield. Microprobe analysis averaged over several sample areas of the single crystal used for diffraction experiments gave an average composition of $K_{1.5}Bi_{2.4}P_{3.2}S_{11.9}$.

$K_9Bi(PS_4)_4$ (III). An ampule containing a mixture of K_2S (0.414 g, 3.8 mmol), Bi (0.1749 g, 0.84 mmol), P (0.1040, 3.4 mmol), and S (0.3078 g, 9.6 mmol) that was prepared in the same manner as **I** was heated to 600 °C over 18 h, held there for 2 h, and then cooled back to room temperature over a period of 8 h. A homogeneous red crystalline ingot that was composed of very moisture-sensitive red plates (∼90%) and greenish gelatinous decomposition products (∼10%) was isolated. The relative amount of the decomposition products increased quickly, and under a light microscope, it was possible to observe regions of the sample decomposing. Microprobe analysis averaged over several sample areas of the single crystal used for diffraction experiments gave an average composition of $K_{9.0}Bi_{0.8}P_{4.3}S_{16.7}$.

Ion Exchange. Because of the large thermal parameters and channel diameters, various sample portions containing **I** were subjected to conditions wherein ion exchange might occur. For solid-state topotactic ion exchange,[39] a ∼0.05 mmol sample portion of compound **I** was ground in an agate mortar and pestle with ∼1.9 mmol AI (A = Rb, Cs) and placed into a 1 cm die. The sample was then pressed into a pellet with ∼4500 kg of force. The pellets were loaded into glass sample vials and placed into an 80 °C oven for 7 days. The products were then washed twice with deionized water, twice with acetone, and once with ether to isolate a black powder.

Solution-phase ion exchange was attempted by combining a ∼0.09 mmol sample portion of compound **I**, ∼3.3 mmol ACl (A = Rb, Cs), and ∼10 mL of deionized water in a glass vial that was

(19) Kanatzidis, M. G. *Chem. Mater.* **1990**, *2*, 353−363.
(20) Kanatzidis, M. G.; Park, Y. *J. Am. Chem. Soc.* **1989**, *111*, 3767−3769.
(21) Kanatzidis, M. G.; Park, Y. *Chem. Mater.* **1990**, *2*, 99−101.
(22) Park, Y. B.; Kanatzidis, M. G. *Angew. Chem., Int. Ed.* **1990**, *29*, 914−915.
(23) McCarthy, T. J.; Kanatzidis, M. G. *Inorg. Chem.* **1995**, *34*, 1257−1267.
(24) Chondroudis, K.; Kanatzidis, M. G. *J. Solid State Chem.* **1998**, *138*, 321−328.
(25) Iordanidis, L.; Bilc, D.; Mahanti, S. D.; Kanatzidis, M. G. *J. Am. Chem. Soc.* **2003**, *125*, 13741−13752.
(26) McCarthy, T. J.; Ngeyi, S. P.; Liao, J. H.; Degroot, D. C.; Hogan, T.; Kannewurf, C. R.; Kanatzidis, M. G. *Chem. Mater.* **1993**, *5*, 331−340.
(27) Iordanidis, L.; Brazis, P. W.; Kyratsi, T.; Ireland, J.; Lane, M.; Kannewurf, C. R.; Chen, W.; Dyck, J. S.; Uher, C.; Ghelani, N. A.; Hogan, T.; Kanatzidis, M. G. *Chem. Mater.* **2001**, *13*, 622−633.
(28) Iordanidis, L.; Schindler, J. L.; Kannewurf, C. R.; Kanatzidis, M. G. *J. Solid State Chem.* **1999**, *143*, 151−162.
(29) Kohatsu, I.; Wuensch, B. J. *Acta Crystallogr., Sect. B* **1976**, *32*, 2401−2409.
(30) McCarthy, T.; Kanatzidis, M. G. *J. Alloys Compd.* **1996**, *236*, 70−85.
(31) Manriquez, V.; Galdamez, A.; Leon, D. R.; Garland, M. T.; Jimenez, M. *Z. Kristallogr.—New Cryst. Struct.* **2003**, *218*, 151−152.
(32) Chung, I.; Karst, A. L.; Weliky, D. P.; Kanatzidis, M. G. *Inorg. Chem.* **2006**, *45*, 2785−2787.
(33) Gave, M.; Malliakas, C. D.; Weliky, D. P.; Kanatzidis, M. G. *Inorg. Chem.* **2007**, *46*, 3632−3644.
(34) Zimmermann, H.; Carpentier, C. D.; Nitsche, R. *Acta Crystallogr., Sect. B* **1975**, *31*, 2003−2006.
(35) Chondroudis, K.; McCarthy, T. J.; Kanatzidis, M. G. *Inorg. Chem.* **1996**, *35*, 840−844.
(36) Chondroudis, K.; Kanatzidis, M. G.; Sayettat, J.; Jobic, S.; Brec, R. *Inorg. Chem.* **1997**, *36*, 5859−5868.
(37) Sayettat, J.; Bull, L. M.; Jobic, S.; Gabriel, J. C. P.; Fourmigue, M.; Batail, P.; Brec, R.; Inglebert, R. L.; Sourisseau, C. *J. Mater. Chem.* **1999**, *9*, 143−153.
(38) Fehér, F. *Handbuch der Präparativen Anorganischen Chemie*; Ferdinand Enke Verlag: Stuttgart, Germany, 1954; Vol. 1, p 280−281.
(39) Chondroudis, K.; Kanatzidis, M. G. *J. Solid State Chem.* **1998**, *136*, 328−332.

Table 1. Crystallographic Data and Experimental and Refinement Details for the Reported Phases

	$K_3Bi_3(PS_4)_4$ (**I**)	$K_{1.5}Bi_{2.5}(PS_4)_3$ (**II**)	$K_9Bi(PS_4)_4$ (**III**)
T, K	298	298	298
cryst syst	tetragonal	monoclinic	orthorhombic
space group	*P*4/*ncc*	$P2/c(\alpha^1/_2\gamma)00$	$P2_12_12$
λ, Å (Mo Kα)	0.071073	0.071073	0.071073
a, Å	21.0116(8)	21.7939(13)	18.306(4)
b, Å	21.0116(8)	8.805(8)	8.926(2)
c, Å	13.3454(10)	10.0301(6)	9.710(2)
α, deg	90	90	90
β, deg	90	90.013(5)	90
γ, deg	90	90	90
q	n/a	0.5**a*** + 0.16**b*** + 0.25**c***	n/a
Z	8	4	2
cryst dimens, mm	0.40 × 0.03 × 0.03	0.10 = 8 × 0.08 × 0.04	0.20 × 0.15 × 0.08
D_{calc}, g/cm^3	3.114	3.583	2.507
μ, mm^{-1}	19.648	24.187	7.992
R_{int}, %	14.2	7.98	10.6
total reflns/ independent	61112/3575	11921/6107	16260/3640
final R/R_w, %[a]	6.7/17.7	6.6/13.3 5.2/12.7 (main) 13.0/24.6 (sat)	5.8/8.9
residual electron density, A^{-3}	4.29 (0.80 Å from Bi(1))	5.27	1.45 (0.45 Å from Bi(2))

[a] $R = \Sigma(|F_o| - |F_c|)/\Sigma|F_o|$. $R_w = [\Sigma w(|F_o| - |F_c|)^2/\Sigma w|F_o|^2]^{1/2}$.

stirred overnight. The resulting black powder was washed twice with deionized water, twice with acetone, and once with ether.

Microprobe analysis of the products from both the solid-state and solution-phase ion-exchange experiments suggested that some exchange had occurred, although the stoichiometric ratio of the elements changed from crystal to crystal. The salt counterion (Cl^- or I^-) was not found in significant amounts, suggesting that the Rb or Cs was in fact in the compound rather than left over from incomplete washing. Powder X-ray diffraction of the powders after solution-based ion exchange matched well with the calculated patterns for **I** while those from the solid-state ion exchange showed a similar pattern of peaks but with a slight shift toward higher 2θ angles.

Powder X-ray Diffraction. All samples were assessed for phase purity using powder X-ray diffraction. Powder patterns were obtained using an INEL CPS 120 powder X-ray diffractometer with monochromatized Cu Kα radiation ($\lambda = 1.540598$ Å) operating at 40 kV and 20 mA equipped with a position-sensitive detector with a 2θ range of 0−120° and calibrated with a LaB_6 standard.

Single-Crystal X-ray Diffraction. Intensity data for single crystals of **I** and **III** were collected on a Bruker SMART platform CCD diffractometer using Mo Kα radiation operating at 40 kV and 40 mA. A full sphere of data was collected, and individual frames were acquired with a 10 s exposure time and a 0.3° omega rotation. The *SMART* software was used for data collection, and the *SAINT* software was used for data extraction and reduction. An analytical absorption correction to the data was performed, and direct methods were used to solve and refine the structures with the *SHELXTL*[40] software package. The details of data collection and refinement are summarized in Table 1.

The crystal structure of compound **I** indicated that the K^+ ion sites within the channels (vide infra) had large thermal parameters, particularly along the channel axes. An attempt was made to model this behavior as a series of sequential cation sites with partial site occupancy, but a significant decrease in reliability statistics was not obtained.

Intensity data for a single crystal of **II** was collected on a Stoe IPDS II diffractometer with Mo Kα radiation operating at 50 kV and 40 mA on with a 34 cm image plate. Individual frames were collected with a 0.5° ω rotation using the *X-AREA* software.[41] The *X-SHAPE* and *X-RED* software packages were used for data extraction and reduction and to apply an analytical absorption correction. The *SHELXTL* and *JANA2000*[42] software packages were used to solve and refine the structure.

The single-crystal X-ray diffraction measurement of **II** was first measured with an exposure time of 2 min and showed reflections belonging to an orthorhombic cell. Analysis of the systematic absences indicated the space group *Pnna*. Direct methods performed with the *SHELX* program package gave a partial solution, and the structure was then refined to yield a satisfying description in terms of interatomic distances and residual electron density values, but with high thermal parameters and residual electron density.

The crystal was then remeasured with a 6 min exposure time. The intention was to check for extra reflections in the diffraction pattern that would reveal additional order in the structure in the form of a structural modulation. Modulated structures have a periodic deviation of atomic positions, site occupancies, or thermal displacement parameters. Therefore, in the structure, translational symmetry of the unit cell is lost and is described in the crystallographic solution as a perturbation to the unit cell. The modulation is manifested in the diffraction pattern because main reflections that correspond to unit cell periodicity are observed along with weaker satellite reflections that correspond to the period of the modulation. These satellite reflections are found in the diffraction pattern along the modulation vector **q** in the reciprocal lattice.[43,44] The reciprocal lattice showed weak first-order satellite reflections, incommensurate with the orthorhombic cell that could be indexed with the one-dimensional (1D) vector $\mathbf{q} = [^1/_4, ^1/_2, 0.16]$.

This modulation vector cannot be combined with orthorhombic symmetry,[45] so the crystal class was lowered and the three-dimensional (3D) space group changed to the highest isomorphic subgroup *P*2/*n*. This space group contains two (3 + 1)-D super space groups, $P2/c(\alpha^1/_2\gamma)00$ and $P2/c(\alpha^1/_2\gamma)0s$, of which only the first gave a useful result after subsequent refinement. Atomic positions were transferred from the *Pnna* model, yielding 22 positions, and the main reflections quickly refined to low residual values ($R_{obs}/R_{all} = 0.034/0.068$) for the average structure. Then modulation waves were applied to the structure to account for satellite reflections. Occupational modulation waves were applied to the mixed K/Bi sites, and positional modulation waves were applied to all atoms in the structure.

The $[PS_4]^{3-}$ tetrahedra were modeled as being internally rigid to decrease the number of crystallographic parameters in the refinement. One $[PS_4]^{3-}$ anion was chosen as the molecular model, and the atomic parameters were first refined individually. The molecular positions and parameters common for the entire molecule were then refined in a rigid body approximation. The final overall

(40) *SMART*, *SAINT*, *SHELXTL*, version 5, *and SADABS*; Bruker Analytical X-ray Instruments, Inc.: Madison, WI, 1998.

(41) *X-AREA*, *X-SHAPE*, and *X-RED*; STOE & Cie GmbH: Darmstadt, Germany, 2004.

(42) Petricek, V.; Dusek, M.; Palatinus, L. *Jana2000. The Crystallographic Computing System*; Institute of Physics: Praha, Czech Republic, 2000.

(43) Evain, M.; Boucher, F.; Gourdon, O.; Petricek, V.; Dusek, M.; Bezdicka, P. *Chem. Mater.* **1998**, *10*, 3068−3076.

(44) Gourdon, O.; Hanko, J.; Boucher, F.; Petricek, V.; Whangbo, M. H.; Kanatzidis, M. G.; Evain, M. *Inorg. Chem.* **2000**, *39*, 1398−1409.

(45) *International Tables of Crystallography*; Kluwer Academic Publishers: Dordrecht, The Netherlands, 2004; Vol. C.

reliability statistics converged to $R/R_w = 6.6/13.3\%$ ($R/R_w = 5.2/12.7\%$ for main reflections and $R/R_w = 13.0/24.6\%$ for satellite reflections) for 11 921 reflections ($I/\sigma(I) > 3$) and 158 parameters.

In an alternative attempt, it was possible to divide the **q** vector into a rational part, $\mathbf{q}^r = [0, {}^1/_2, 0]$, and an irrational part, $\mathbf{q}^i = [0.25, 0, 0.16]$. The rational part could then be excluded by applying a centering condition. This resulted in the super space group $X2/c(\alpha 0 \gamma)00$, where X corresponded to the (3 + 1)-D centering [0, ${}^1/_2$, 0, ${}^1/_2$]. However, this required that the b axis was doubled, and so the overall gain in such a description for an already large unit cell was limited and was therefore not considered.

Only 35% of the satellite reflections met the observation criteria of $I > 3\sigma$, and the absence of higher orders made the modulation difficult to model precisely. The final residual values are about 13% for the satellites, but the low overall R value (6.61%) reflects the minor effect of the modulation on the structure. The exchange of Bi for K in two different sites can apparently be made smoothly, with no drastic effects on the rest of the structure and thus the weak intensity of the satellite reflections.

Electron Microscopy. A JEOL JSM-35C scanning electron microscope equipped with a Tracor Northern energy dispersive spectroscopy detector was used for quantitative microprobe analysis. Data were collected using an accelerating voltage of 25 kV and a collection time of 60 s, and the results were averaged over several sample areas.

Differential Thermal Analysis. Differential thermal analyses were performed with a Shimadzu DTA-50 thermal analyzer. A ground sample weighing ~25 mg was sealed in a quartz ampule under reduced pressure. An equivalent mass of alumina was sealed in an identical ampule to serve as a reference. The samples were heated to 850 °C at a rate of 10 °C/min, cooled to 150 °C at a rate of 10 °C/min, reheated to 850 °C at a rate of 10 °C/min, and then cooled to room temperature at a rate of 10 °C/min.

Raman Spectroscopy. Raman (750−100 cm^{-1}) spectra were collected using a BIO-RAD FT spectrometer equipped with a Spectra-Physics Topaz T10-106c 1.064 nm YAG laser and a Ge detector. Samples were ground into a fine powder and loaded into fused silica tubes, and 64 scans were averaged.

Solid-State NMR. Room-temperature ^{31}P solid-state NMR spectra were collected on a 9.4 T spectrometer (Varian Infinity Plus) using a double-resonance magic-angle spinning probe. Samples were spun at frequencies ranging from 5 to 15 kHz in 4 mm outer diameter zirconia rotors and a ~50 μL sample volume. Bloch decay spectra were taken with a 4 μs 90° pulse (calibrated and referenced to 85% H_3PO_4 at 0 ppm) and relaxation delays ranging from 10 to 5000 s. Each spectrum was processed with 10 Hz line broadening and up to a 10th order polynomial baseline correction.

The longitudinal relaxation time (T_1) of each compound was estimated by fitting to the equation

$$S(t) = S_0(1 - e^{-\tau/T_1}) \quad (1)$$

where τ is the experimental delay time, $S(\tau)$ is the experimental signal intensity, and S_0 is a fitting parameter representing the signal intensity at $\tau = \infty$.[46]

Results and Discussion

Synthetic Reactions. The compounds **II** and **III** were produced by the direct stoichiometric reaction of K_2S, Bi, P, and S; however, we were not able to prepare **I** as the dominant compound without additional K_2S_x in the reaction. Presumably, the K_2S_x acted as a flux in which **I** could grow. If K_xS_y was not added, **II** was produced in high yields. When the value of x in K_2S_x was decreased, $K_3Bi(PS_4)_2$[30] was produced along with a significant amount of Bi_2S_3. The synthesis of **III** required even more basic K_2S_x compositions. In syntheses of compound **I**, we always observed compound **II** and $K_3Bi(PS_4)_2$ present in detectable quantities.

Compounds **I** and **II** were stable in ambient conditions, but **III** was highly moisture sensitive and decomposed rapidly when exposed to air. This reactivity can be attributed to the presence of the highly charged $[Bi(PS_4)_4]^{9-}$ molecular anion in the structure.[47]

In an attempt to prepare pure **I**, a melt of the same composition was quenched in ice water. The intention was to kinetically trap a solid with the correct stoichiometry which could then be annealed at a given temperature to produce crystalline **I**. The resultant solid was an amorphous

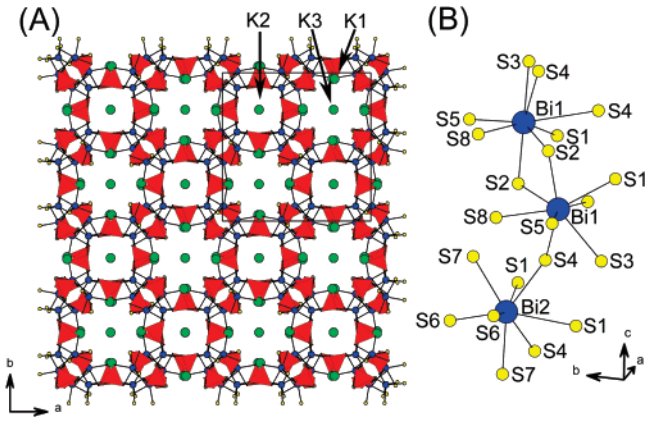

Figure 1. (A) **I** viewed down the [001] axis showing the large channels that are occupied by K^+ ions. (B) An undulating Bi_3S_{12} chain that forms the walls of the tunnels.

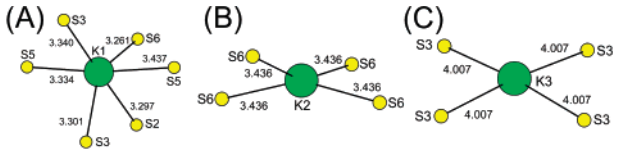

Figure 2. Coordination environments of (A) K(1), (B) K(2), and (C) K(3) ions in **I**.

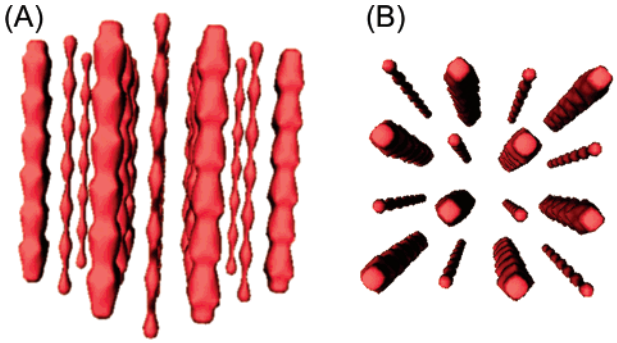

Figure 3. Void space representation of **I** showing the relative sizes and contours of each of the channels viewed (A) perpendicular to [001] and (B) parallel to [001].

(46) Canlas, C. G.; Muthukumaran, R. B.; Kanatzidis, M. G.; Weliky, D. P. *Solid State Nucl. Magn. Reson.* **2003**, *24*, 110−122.

(47) Chondroudis, K.; Kanatzidis, M. G. *Inorg. Chem. Commun.* **1998**, *1*, 55−57.

Table 2. Selected Bond Lengths (Å) and Angles (deg) for **I** with Standard Uncertainties in Parentheses[a]

Bi1−S5	2.707(5)	S5−Bi1−S2	82.99(13)	S3^{viii}−K1−S1^{vii}	139.5(2)
Bi1−S2	2.791(4)	S5−Bi1−S8	71.86(15)	S5^{ix}−K1−S1^{vii}	118.42(16)
Bi1−S8	2.844(5)	S2−Bi1−S8	84.50(14)	S3^{ix}−K1−S1^{vii}	57.21(13)
Bi1−S1	2.888(5)	S5−Bi1−S1	95.13(16)	S5−K1−S1^{vii}	56.77(13)
Bi1−S3	3.006(5)	S2−Bi1−S1	70.64(12)	S7^{viii}−K1−S1^{vii}	134.72(19)
Bi1−S2^{i}	3.026(4)	S8−Bi1−S1	153.38(15)	S6^{x}−K2−S6^{xi}	153.05(15)
Bi1−S4^{ii}	3.091(5)	S5−Bi1−S3	80.15(13)	S6^{x}−K2−S6^{iv}	77.62(15)
Bi2−S6	2.770(4)	S2−Bi1−S3	142.73(12)	S6^{xi}−K2−S6^{iv}	108.84(15)
Bi2−S6^{i}	2.770(4)	S8−Bi1−S3	120.58(15)	S6^{x}−K2−S6^{xii}	108.84(15)
Bi2−S7	2.870(4)	S1−Bi1−S3	78.04(13)	S6^{xi}−K2−S6^{xii}	77.62(15)
Bi2−S7^{i}	2.870(4)	S5−Bi1−S2^{i}	136.37(13)	S6^{iv}−K2−S6^{xii}	153.04(15)
Bi2−S4	2.916(5)	S2−Bi1−S2^{i}	78.40(12)	S6^{x}−K2−S8^{xiii}	64.29(11)
Bi2−S4^{i}	2.916(5)	S8−Bi1−S2^{i}	67.38(13)	S6^{xi}−K2−S8^{xiii}	103.24(11)
		S1−Bi1−S2^{i}	114.76(14)	S6^{iv}−K2−S8^{xiii}	141.55(11)
K1−S6^{vii}	3.259(7)	S3−Bi1−S2^{i}	134.64(11)	S6^{xii}−K2−S8^{xiii}	54.66(11)
K1−S2	3.296(6)	S5−Bi1−S4^{ii}	116.36(15)	S6^{x}−K2−S8^{xiv}	103.24(11)
K1−S3^{viii}	3.302(7)	S2−Bi1−S4^{ii}	150.64(13)	S6^{xi}−K2−S8^{xiv}	64.29(11)
K1−S5^{ix}	3.334(7)	S8−Bi1−S4^{ii}	81.44(14)	S6^{iv}−K2−S8^{xiv}	54.66(11)
K1−S3^{ix}	3.340(7)	S1−Bi1−S4^{ii}	125.06(14)	S6^{xii}−K2−S8^{xiv}	141.55(11)
K1−S5	3.437(7)	S3−Bi1−S4^{ii}	65.78(12)	S8^{xiii}−K2−S8^{xiv}	127.89(16)
K1−S7^{viii}	3.663(8)	S2^{i}−Bi1−S4^{ii}	72.42(12)	S6^{x}−K2−S8^{ii}	141.55(11)
K1−S1^{vii}	3.703(7)	S6−Bi2−S6^{i}	102.1(2)	S6^{xi}−K2−S8^{ii}	54.66(11)
K2−S6^{x}	3.437(5)	S6−Bi2−S7	70.95(13)	S6^{iv}−K2−S8^{ii}	64.29(11)
K2−S6^{xi}	3.437(5)	S6^{i}−Bi2−S7	85.25(15)	S6^{xii}−K2−S8^{ii}	103.24(11)
K2−S6^{iv}	3.437(5)	S6−Bi2−S7^{i}	85.25(15)	S8^{xiii}−K2−S8^{ii}	154.09(15)
K2−S6^{xii}	3.437(5)	S6^{i}−Bi2−S7^{i}	70.95(13)	S8^{xiv}−K2−S8^{ii}	59.10(16)
K2−S8^{xiii}	3.850(6)	S7−Bi2−S7^{i}	142.0(2)	S6^{x}−K2−S8^{xv}	54.66(11)
K2−S8^{xiv}	3.850(6)	S6−Bi2−S4	91.87(15)	S6^{xi}−K2−S8^{xv}	141.55(11)
K2−S8^{ii}	3.850(6)	S6^{i}−Bi2−S4	134.95(13)	S6^{iv}−K2−S8^{xv}	103.24(11)
K2−S8^{xv}	3.850(6)	S7−Bi2−S4	139.52(15)	S6^{xii}−K2−S8^{xv}	64.29(11)
K3−S3	4.006(9)	S7^{i}−Bi2−S4	67.81(13)	S8^{xiii}−K2−S8^{xv}	59.10(16)
K3−S3^{v}	4.006(9)	S6−Bi2−S4^{i}	134.94(13)	S8^{xiv}−K2−S8^{xv}	154.09(15)
K3−S3^{vii}	4.006(9)	S6^{i}−Bi2−S4^{i}	91.87(15)	S8^{ii}−K2−S8^{xv}	127.89(16)
K3−S3^{xvi}	4.006(9)	S7−Bi2−S4^{i}	67.81(13)	S3−K3−S3^{v}	89.8(2)
K3−K1^{xvii}	4.40(2)	S7^{i}−Bi2−S4^{i}	139.52(15)	S3−K3−S3^{vii}	89.8(2)
K3−K1^{iii}	4.40(2)	S4−Bi2−S4^{i}	107.97(19)	S3^{v}−K3−S3^{vii}	174.(4)
K3−K1^{ii}	4.40(2)			S3−K3−S3^{xvi}	174.(4)
K3−K1^{xi}	4.40(2)	S6^{vii}−K1−S2	74.07(15)	S3^{v}−K3−S3^{xvi}	89.8(2)
K3−S5^{v}	5.29(7)	S6^{vii}−K1−S3^{viii}	134.57(19)	S3^{vii}−K3−S3^{xvi}	89.8(2)
		S2−K1−S3^{viii}	60.85(13)	S3−K3−S5^{v}	56.8(8)
P1−S3^{viii}	2.020(6)	S6^{vii}−K1−S5^{ix}	109.81(19)	S3^{v}−K3−S5^{v}	44.1(7)
P1−S1	2.031(6)	S2−K1−S5^{ix}	116.74(19)	S3^{vii}−K3−S5^{v}	132.(2)
P1−S4	2.044(6)	S3^{viii}−K1−S5^{ix}	86.98(16)	S3^{xvi}−K3−S5^{v}	119.7(18)
P1−S2	2.071(6)	S6^{vii}−K1−S3^{ix}	108.58(18)	K1^{xvii}−K3−S5^{v}	157.(3)
P2−S7^{vii}	2.015(6)	S2−K1−S3^{ix}	174.7(2)	K1^{iii}−K3−S5^{v}	101.3(9)
P2−S8	2.022(7)	S3^{viii}−K1−S3^{ix}	116.8(2)	K1^{ii}−K3−S5^{v}	38.9(5)
P2−S6^{vii}	2.063(6)	S5^{ix}−K1−S3^{ix}	67.02(14)	K1^{xi}−K3−S5^{v}	87.0(7)
P2−S5	2.071(7)	S6^{vii}−K1−S5	61.52(14)		
		S2−K1−S5	65.47(13)	S3^{viii}−P1−S1	113.4(3)
		S3^{viii}−K1−S5	101.51(17)	S3^{viii}−P1−S4	109.2(3)
		S5^{ix}−K1−S5	170.7(2)	S1−P1−S4	109.4(3)
		S3^{ix}−K1−S5	111.46(18)	S3^{viii}−P1−S2	109.5(3)
		S6^{vii}−K1−S7^{viii}	71.44(16)	S1−P1−S2	106.4(3)
		S2−K1−S7^{viii}	66.27(14)	S4−P1−S2	108.8(3)
		S3^{viii}−K1−S7^{viii}	84.98(17)	S7^{vii}−P2−S8	110.6(3)
		S5^{ix}−K1−S7^{viii}	57.34(14)	S7^{vii}−P2−S6^{vii}	106.8(3)
		S3^{ix}−K1−S7^{viii}	118.75(18)	S8−P2−S6^{vii}	110.9(3)
		S5−K1−S7^{viii}	119.20(18)	S7^{vii}−P2−S5	111.1(3)
		S6^{vii}−K1−S1^{vii}	69.13(15)	S8−P2−S5	105.5(3)
		S2−K1−S1^{vii}	120.95(17)	S6^{vii}−P2−S5	112.0(3)

[a] Symmetry codes: (i) 0.5 + *y*, −0.5 + *x*, 0.5 − *z*; (ii) 0.5 − *y*, 0.5 − *x*, 0.5 + *z*; (iii) *x*, 0.5 − *y*, 0.5 + *z*; (iv) 0.5 + *y*, −*x*, 1 − *z*; (v) *y*, 0.5 − *x*, *z*; (vi) 1 − *x*, −0.5 + *y*, 0.5 − *z*; (vii) 0.5 − *y*, *x*, *z*; (viii) 0.5 − *y*, 0.5 − *x*, −0.5 + *z*; (ix) *x*, 0.5 − *y*, −0.5 + *z*; (x) *x*, −0.5 − *y*, 0.5 + *z*; (xi) 0.5 − *x*, *y*, 0.5 + *z*; (xii) −*y*, −0.5 + *x*, 1 − *z*; (xiii) −0.5 + x, −0.5 + *y*, 1 − *z*; (xiv) 1 − *x*, −*y*, 1 − *z*; (xv) *y*, −1 + *x*, 0.5 + *z*; (xvi) 0.5 − *x*, 0.5 − *y*, *z*; (xvii) *y*, *x*, 0.5 + *z*; (xviii) 1 − *x*, −*y*, −*z*.

glass as confirmed with powder X-ray diffraction. Differential thermal analysis of the glass indicated the onset of crystallization at about 320 °C. The sample was then carefully annealed at 320 °C, but the resulting product was found to be $K_{1.5}Bi_{2.5}(PS_4)_3$ with no evidence for compound **I**. It is likely that compound **I** is stabilized by the presence of a K_2S_x flux and is just not kinetically stable.

Structure Description. $K_3Bi_3(PS_4)_4$ (I). This compound has a complex 3D $[Bi_3(PS_4)_4]^{3-}$ anionic framework with infinite parallel tunnels running through it (Figure 1A). The tunnels are parallel to the *c* axis and are filled with charge-balancing K^+ ions. There are two types of tunnels in the structure. Type I tunnels are located at ($^3/_4$, $^1/_4$) in the *ab* plane and have K(2) atoms in their center. Type II tunnels

are located at ($^1/_4$, $^3/_4$) and accommodate the K(1) and K(3) atoms. Each tunnel type is surrounded by four other tunnels of the other type.

The K(1) atoms are located at the tunnel edge, interacting with S atoms with an average K−S bond length of 3.33 Å (Figure 2A). The K(3) central axes are located at the tunnel center with K−S distances of ∼4 Å (Figure 2C). The K(3) atoms are located in the same tunnel as the K(1) atoms, but instead of being placed on the edge, they are situated at the center of the tunnel. The K(2) site is distorted square planar with K(2)−S interactions of 3.436(5) Å (Figure 2B). The K2 and K3 ion sites had large thermal parameters, and the possibility of this being due to long-range ordering was considered. Zone photos obtained with X-ray diffraction using relatively long exposure times did not reveal any evidence for weak satellite reflections, and therefore, significant contributions from a modulation are unlikely. Therefore, the large thermal parameters are probably due to static positional disorder of the K^+ atoms in the oversized tunnels. The greatest displacement in each case was along the (001) axis, which suggests the possibility of high ion mobility within the tunnels.

The size and shape of the two types of tunnels were approximated by plotting the isosurface that lies between the framework atoms (Figure 3).[48] The smaller tunnel (type I) has a diameter of ∼3.1 Å, and the larger one (type II) has a diameter of ∼4.4 Å. The two types of tunnels do not seem to be connected by holes of significant girth.

The $[Bi_3(PS_4)_4]^{3-}$ framework itself is built from undulating chains of Bi−S polyhedra. If the P atoms are ignored, the structure is made of pairs of parallel Bi_3S_{12} chains (Figure 1B). In each chain, the distorted Bi polyhedra share corners or edges. Bi(1) is pseudo eight-coordinate and is chelated by three $[PS_4]^{3-}$ anions. Seven of the Bi−S distances are relatively short, with an average bond length of 2.91 Å. The remaining interaction is between Bi(1) and S(4) at a distance at 3.451(6) Å and is likely elongated due to the stereochemically active so-called $6s^2$ "lone pair" of electrons on Bi. The stereochemical activity presumably arises from an interaction between the Bi 6s valence electrons and the chalcogen valence p orbitals that results in an asymmetric distribution of the former.[49] Two Bi(1) atoms are bridged by S atoms with Bi(1)−S(2) distances of 2.791(4) and 3.026(4) Å. Bi(1) is also connected to Bi(2) by a bridging S atom. Bi(2) is pseudo eight-coordinate, is chelated by three $[PS_4]^{3-}$ anions, and forms the inner wall of the tunnel. Six of the Bi−S distances are relatively short, with an average bond length of 2.85 Å. The putative lone pair of electrons on Bi is suggested by the elongated Bi(2)−S(1) length of 3.384(6) Å. The action of the four-fold axis on the chain of $[Bi_3(PS_4)_4]^{3-}$ forms it into the tunnel. Selected bond lengths and angles are displayed in Table 2.

$K_{1.5}Bi_{2.5}(PS_4)_3$ (II). The structure of this compound is incommensurately modulated, and it has a 3D framework

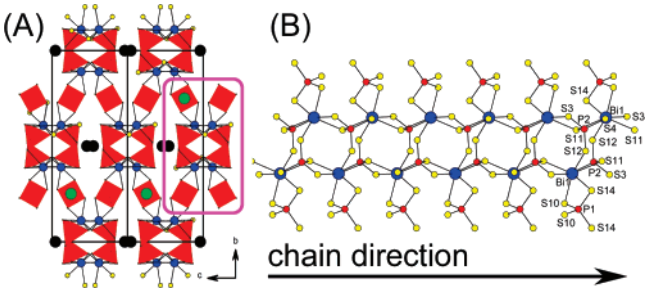

Figure 4. (A) 3D approximant structure of **II** as viewed down [100] showing the assembly of the chains centered at $^1/_2$ the [010] and [001] axes and the assembly of "$Bi_2(PS_4)_4$" chains, emphasized in a rectangular outline. (B) An individual "$Bi_2(PS_4)_4$" chain as viewed down the [001] axis.

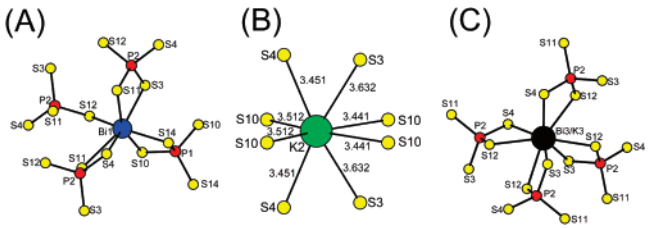

Figure 5. The coordination environment of (A) Bi(1), (B) K(2), and (C) the K(3)/Bi(3) mixed site in **II**.

structure (Figure 4A). Compound **II** adopts the monoclinic super spacegroup $P2/c(\alpha^1/_2\gamma)$ with the modulation vector having **a***, **b***, and **c*** components. The related compound $K_3Ce_2(PS_4)_3$[50] was also found to be modulated and has the super spacegroup $C2/c(\alpha 0\gamma)$.

In the orthorhombic model before the modulation was introduced, there was one Bi^{3+} site (Bi(1)), one K^+ site (K(2)), and one site that could only be described as being mixed between K^+ and Bi^{3+} (K(3)/Bi(3)) with a 50% occupancy (Figure 5). The framework is built of interconnected "$Bi_2(PS_4)_4$" double chains (Figure 4B). Bi(2) atoms are bridged by S(11) along the *a* axis in a zigzag pattern to form a single chain. Two chains are connected by a P(2)-centered $[PS_4]^{3-}$ ion to form the double chains. Neighboring double chains are then interconnected by bridging P(1)-centered $[PS_4]^{3-}$ ions and by K(3) ions that undulate down the *a* axis. The K(3)/Bi(3) and K(4)/Bi(4) mixed sites are located in the channels between the chains. Selected bond lengths and angles are given in Table 3.

In the case of compounds **I**, **III**, $KBiP_2S_7$,[26,30] $KBiP_2S_6$,[31] and $K_3Bi(PS_4)_2$,[30] no cation site disorder was observed, and therefore, the possibility of a structural modulation rather than random disorder was considered. X-ray diffraction data with a longer exposure time was subsequently collected to look for satellite reflections indicating long-range order. The data revealed first-order reflections that could be indexed with the modulation vector $\mathbf{q} = 0.25\mathbf{a}^* + 0.5\mathbf{b}^* + 0.16\mathbf{c}^*$. Higher order satellite reflections were not observed.

Upon transformation to $P2/c(\alpha^1/_2\gamma)00$, the mixed K/Bi position from the orthorhombic model was split into two positions (K(3)/Bi(3)) and K(4)/Bi(4)), and all thermal displacement parameters were reasonable. The application of an occupational modulation indicated that the modula-

(48) Nagy, T. F.; Mahanti, S. D.; Dye, J. L. *Zeolites* **1997**, *19*, 57−64.
(49) Stoltzfus, M. W.; Woodward, P. M.; Seshadri, R.; Klepeis, J. H.; Bursten, B. *Inorg. Chem.* **2007**, *46*, 3839−3850.
(50) Gauthier, G.; Evain, M.; Jobic, S.; Brec, R. *Solid State Sci.* **2002**, *4*, 1361−1366.

Table 3. Selected Bond Lengths (Å) and Angles (deg) for **II**, with Standard Uncertainties in Parentheses

distance	average	min	max				
Bi1−S1a	2.712(5)	2.704(6)	2.719(6)		S1a−P1a−S2a	110.2(2)	
Bi1−S1b	2.797(5)	2.740(5)	2.852(5)		S1a−P1a−S3a	107.3(2)	
Bi1−S3a	2.715(5)	2.689(5)	2.740(5)		S1a−P1a−S4a	108.9(2)	
Bi1−S2b	3.193(5)	3.020(5)	3.371(5)		S2a−P1a−S3a	111.1(2)	
Bi1−S3b	2.829(5)	2.796(5)	2.866(5)		S2a−P1a−S4a	109.1(2)	
Bi1−S3b	3.006(5)	2.970(5)	3.046(5)		S3a−P1a−S4a	110.2(2)	
Bi1−S4b	2.895(5)	2.876(5)	2.919(5)				
Bi2−S2a	2.720(6)	2.717(5)	2.724(5)	K4−S1c	3.063(5)	3.012(5)	3.107(5)
Bi2−S4a	2.729(5)	2.724(5)	2.735(5)	K4−S1c	3.064(5)	3.011(5)	3.108(5)
Bi2−S1c	2.797(5)	2.763(5)	2.833(5)	K4−S2c	3.141(5)	3.106(5)	3.169(5)
Bi2−S2c	3.200(5)	3.155(5)	3.241(5)	K4−S2c	3.140(5)	3.106(5)	3.170(5)
Bi2−S3c	2.831(5)	2.821(5)	2.839(5)	K4−S4c	2.967(5)	2.952(5)	2.981(5)
Bi2−S3c	3.004(5)	2.992(5)	3.015(5)	K4−S4c	3.072(5)	3.056(5)	3.087(5)
Bi2−S4c	2.892(5)	2.878(5)	2.907(5)	K4−S4c	2.968(5)	2.951(5)	2.982(5)
				K4−S4c	3.073(5)	3.056(5)	3.087(5)
Bi3−S1b	3.069(5)	3.043(5)	3.099(5)				
Bi3−S1b	3.073(5)	3.043(5)	3.098(5)	K1−S1a	3.419(7)	3.382(7)	3.450(7)
Bi3−S2b	3.132(5)	3.036(5)	3.223(5)	K1−S1a	3.487(7)	3.465(7)	3.506(7)
Bi3−S2b	3.126(5)	3.036(5)	3.223(5)	K1−S2a	3.400(7)	3.377(7)	3.421(7)
Bi3−S4b	2.974(5)	2.899(5)	3.055(5)	K1−S2a	3.499(7)	3.452(7)	3.542(7)
Bi3−S4b	3.063(5)	3.007(5)	3.124(5)	K1−S1b	3.604(8)	3.597(8)	3.612(8)
Bi3−S4b	2.980(5)	2.899(5)	3.056(5)	K1−S2b	3.452(8)	3.385(8)	3.531(8)
Bi3−S4b	3.067(5)	3.006(5)	3.124(5)	K1−S1c	3.600(8)	3.554(8)	3.649(8)
				K1−S2c	3.451(9)	3.428(9)	3.476(9)
K3−S1b	3.069(5)	3.043(5)	3.099(5)				
K3−S1b	3.073(5)	3.043(5)	3.098(5)	P1a−S1a	2.062(5)	2.062(5)	2.062(5)
K3−S2b	3.132(5)	3.036(5)	3.223(5)	P1a−S2a	2.035(5)	2.035(5)	2.035(5)
K3−S2b	3.126(5)	3.036(5)	3.223(5)	P1a−S3a	2.034(6)	2.034(6)	2.035(5)
K3−S4b	2.974(5)	2.899(5)	3.055(5)	P1a−S4a	2.045(6)	2.044(6)	2.045(5)
K3−S4b	3.063(5)	3.007(5)	3.124(5)				
K3−S4b	2.980(5)	2.899(5)	3.056(5)				
K3−S4b	3.067(5)	3.006(5)	3.124(5)				
Bi4−S1c	3.063(5)	3.012(5)	3.107(5)				
Bi4−S1c	3.064(5)	3.011(5)	3.108(5)				
Bi4−S2c	3.141(5)	3.106(5)	3.169(5)				
Bi4−S2c	3.140(5)	3.106(5)	3.170(5)				
Bi4−S4c	2.967(5)	2.952(5)	2.981(5)				
Bi4−S4c	3.072(5)	3.056(5)	3.087(5)				
Bi4−S4c	2.968(5)	2.951(5)	2.982(5)				
Bi4−S4c	3.073(5)	3.056(5)	3.087(5)				

tion between K(4) and Bi(4) had a small amplitude whereas the modulation between K(3) and B(3) had a larger amplitude (Figure 6). A summary of the applied modulation waves is displayed in Table 4. After taking into account this occupational modulation, the stoichiometry refined to $K_{1.47}Bi_{2.49}P_3S_{12}$, in close agreement with the microprobe analysis. A positional modulation was then applied to all atoms in the structure as well as to the rigid $[PS_4]^{3-}$ units. The largest positional deviations (∼0.1 Å) were observed in Bi(1) and the $[PS_4]^{3-}$ tetrahedron closest to it. The modulation over several unit cells is displayed in Figure 7.

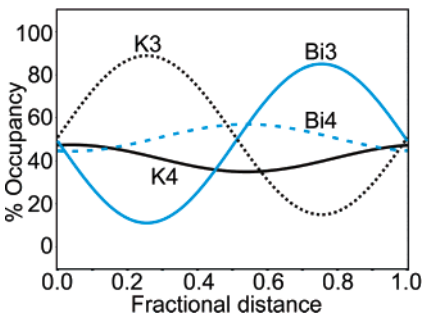

Figure 6. Percent occupancies of the complementary modulated sites K(3)/Bi(3) and K(4)/Bi(4) in **II** with the ordinate representing the fractional distance along the modulation axis.

$K_9Bi(PS_4)_4$ (III). Compound **III** has discreet molecules of $[Bi(PS_4)_4]^{9-}$ and is structurally related to $Rb_9Ce(PS_4)_4$[47] and $K_9Ce(PS_4)_4$[51] (Figure 8A). The $[Bi(PS_4)_4]^{9-}$ molecules are arranged in layers parallel to the *bc* plane with the K^+ atoms in between. The molecular complex $[Bi(PS_4)_4]^{9-}$ anion features two chelating $[PS_4]^{3-}$ ligands and two monodentate $[PS_4]^{3-}$ anions (Figure 8B). The average Bi−S distance is 2.86 Å. The next-nearest S atoms on the monodentate $[PS_4]^{3-}$ are 3.708(4) Å from Bi. K^+ is in a distorted bicapped octahedral site with K−S distances averaging 3.38 Å (Figure 9). The P−S distances average 2.04 Å. Selected bond lengths and angles are displayed in Table 5.

Structural Dimensionality. To place the stoichiometry and the dimensionality of the compounds in a greater context, it is useful to consider each of the known $(PS_4)^{3-}$-containing compounds as a member of the homologous series $(K_3PS_4)_n$-$(BiPS_4)_m$ (Scheme 1).[31,34−36] In this formalism, the compound $BiPS_4$ is a member of the series with an *n*/*m* ratio of 0. $BiPS_4$ has a dense 3D framework. As the *n*/*m* ratio increases, the dimensionality of the framework is reduced. Thus, the Bi/P/S framework in **II** at an *n*/*m* ratio of 0.20 is also 3D but the framework architecture is relatively open with tunnels accommodating K ions. When the *n*/*m* ratio is increased to

Table 4. Modulation Parameters for **II**

Occupation Waves

	U_{cos}	U_{sin}
Bi3	−0.0512(7)	0.366(5)
K3	0.0512(7)	−0.366(5)
Bi4	−0.062(4)	0.0083(6)
K4	0.062(4)	−0.0083(6)

Displacement Waves

		U_{cos}	U_{sin}			U_{cos}	U_{sin}
	x	−0.00111(5)	−0.00083(5)		*x*	0.0003(2)	0.0010(2)
Bi1	*y*	−0.01021(9)	−0.00568(10)	S2a	*y*	0.0001(4)	0.0004(3)
	z	0.00604(9)	0.00927(8)		*z*	0.0030(4)	0.0090(3)
	x	0.00004(5)	0.00002(5)		*x*	−0.00019(18)	−0.00188(17)
Bi2	*y*	0.00013(11)	−0.00115(11)	S3a	*y*	−0.0022(5)	−0.0072(5)
	z	−0.00096(10)	−0.00114(10)		*z*	0.0028(4)	0.0110(4)
	x	0.00107(11)	0.000150(15)		*x*	−0.00051(18)	−0.00234(17)
Bi3	*y*	0.00108(4)	−0.0077(3)	S4a	*y*	0.0008(5)	−0.0028(5)
	z	0.00160(19)	0.00022(3)		*z*	0.0026(4)	0.0030(4)
	x	0.00107(11)	0.000150(15)		*x*	−0.0015(2)	−0.00105(19)
K3	*y*	0.00108(4)	−0.0077(3)	S1b	*y*	−0.0030(5)	−0.0028(4)
	z	0.00160(19)	0.00022(3)		*z*	0.0043(4)	0.0095(3)
	x	0.000081(16)	0.00061(12)		*x*	−0.00153(19)	−0.00260(18)
Bi4	*y*	−0.0025(2)	0.00033(3)	S2b	*y*	−0.0039(5)	−0.0072(4)
	z	−0.00025(3)	−0.00191(19)		*z*	0.0045(4)	0.0105(3)
	x	0.000081(16)	0.00061(12)		*x*	−0.00183(18)	−0.00083(18)
K4	*y*	−0.0025(2)	0.00033(3)	S3b	*y*	−0.0035(4)	−0.0032(4)
	z	−0.00025(3)	−0.00191(19)		*z*	0.0050(4)	0.0119(4)
	x	−0.0009(3)	−0.0001(3)		*x*	−0.00148(18)	−0.00180(18)
K1	*y*	0.0003(7)	0.0060(7)	S4b	*y*	−0.0043(5)	−0.0034(4)
	z	0.0035(6)	0.0030(6)		*z*	0.0045(4)	0.0063(4)
	x	−0.00034(15)	−0.00102(14)		*x*	−0.00089(19)	−0.0008(2)
P1a	*y*	−0.0005(3)	−0.0026(3)	S1c	*y*	0.0028(5)	0.0030(5)
	z	0.0027(2)	0.0071(2)		*z*	−0.0009(4)	−0.0016(4)
	x	−0.00158(13)	−0.00158(12)		*x*	−0.00073(19)	−0.00082(19)
P1b	*y*	−0.0037(3)	−0.0042(3)	S2c	*y*	0.0033(5)	0.0021(5)
	z	0.0045(3)	0.0096(2)		*z*	−0.0011(4)	−0.0014(4)
	x	−0.00072(13)	−0.00073(13)		*x*	−0.00043(18)	−0.00042(18)
P1c	*y*	0.0026(3)	0.0023(3)	S3c	*y*	0.0025(4)	0.0024(4)
	z	−0.0011(2)	−0.0013(2)		*z*	−0.0014(4)	−0.0008(4)
	x	−0.0009(2)	−0.0008(2)		*x*	−0.00084(18)	−0.00085(18)
S1a	*y*	−0.0007(4)	−0.0009(3)	S4c	*y*	0.0019(4)	0.0016(4)
	z	0.0025(4)	0.0051(3)		*z*	−0.0010(4)	−0.0013(4)

0.33, an even more open 3D framework compound **I** is stabilized. A further increase of the *n*/*m* ratio to 1 gives the 1D chains of $K_3Bi(PS_4)_2$, and the largest *n*/*m* ratio of 3 gives the molecular **III**. As the *n*/*m* ratio is increased, the 3D covalent $BiPS_4$ framework is dismantled by dilution with ionic K_3PS_4 that lowers the dimensionality of the resultant compound. The dimensional reduction of a covalent framework can be a practical formalism in studying structural evolution in solids and has been discussed earlier as a means to controlling the structures and properties of materials.[52,53] For example, the incorporation of K_2S into HgS amounts to the introduction of S^{2-} atoms in the diamond lattice of HgS and the generation of anionic low-dimensional $[Hg_xS_y]^{n-}$ frameworks. In essence, the dense packed lattice of the parent compound is "diluted" with S^{2-} atoms, which progressively dismantle it. The K^+ ion acts as a "noninterfering" counterion. A chemical homology created in this way is of type $(K_2S)_m(HgS)_n$.[54] Other such examples in chalcogenides include $(A_2Q)_m(CdQ)_n$[55] and $(A_2Q)_m(Bi_2Q_3)_n$[26,56] systems.

Raman Spectroscopy. Raman spectra were collected for each of the title compounds (Figure 10). In each case, a peak at ∼410 cm^{-1} was observed, which is attributed to the $[PS_4]^{3-}$ symmetrical stretch.[57] Also, each spectrum showed a band of overlapping peaks from ∼150 to ∼300 cm^{-1} that shows similarities to the Raman spectrum of Bi_2S_3, suggesting that those peaks can be attributed to various Bi−S vibrational modes. A small amount of highly crystalline material Bi_2S_3 may dominate the Raman spectrum even though it is present in small quantities.

Compound **II** also showed a third intense region of features with peaks centered at 519, 538, and 562 cm^{-1} (Figure 10B). Despite the presence of some of compound **II** in the sample used to collect a Raman spectrum of compound **I**, this region of features was not evident for the NMR spectrum of **I** (Figure 10A). At present, the exact assignment of these modes that appear to be unique to compound **II** is not

(51) Gauthier, G.; Jobic, S.; Danaire, V.; Brec, R.; Evain, M. *Acta Crystallogr., Sect. C: Cryst. Struct. Commun.* **2000**, *56*, 117.
(52) Tulsky, E. G.; Long, J. R. *Chem. Mater.* **2001**, *13*, 1149−1166.
(53) Long, J. R.; McCarty, L. S.; Holm, R. H. *J. Am. Chem. Soc.* **1996**, *118*, 4603−4616.
(54) Axtell, E. A.; Park, Y.; Chondroudis, K.; Kanatzidis, M. G. *J. Am. Chem. Soc.* **1998**, *120*, 124−136.
(55) Axtell, E. A.; Liao, J. H.; Pikramenou, Z.; Kanatzidis, M. G. *Chemistry—Eur. J.* **1996**, *2*, 656−666.
(56) Kanatzidis, M. G.; McCarthy, T. J.; Tanzer, T. A.; Chen, L. H.; Iordanidis, L.; Hogan, T.; Kannewurf, C. R.; Uher, C.; Chen, B. X. *Chem. Mater.* **1996**, *8*, 1465−1474.
(57) Evenson, C. R.; Dorhout, P. K. *Inorg. Chem.* **2001**, *40*, 2884−2891.

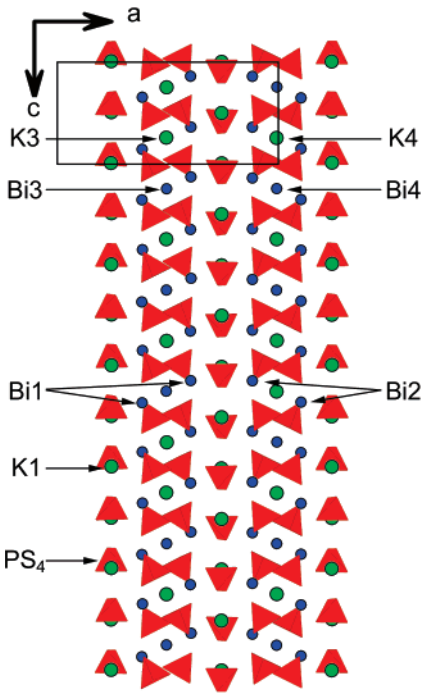

Figure 7. View of **II** down the *b* axis, showing how the K and Bi atoms interchange differently along the *c* axis for the K3/Bi3 and K4/Bi4 pairs. The subcell is displayed in black lines.

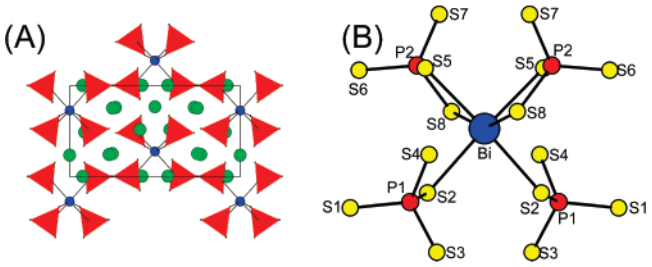

Figure 8. (A) View down [010] of **III** and (B) a view of an individual molecule of $[Bi(PS_4)]^{9-}$.

complete, but it is possible that the metal−sulfur bonds would give rise to features in this region. Perhaps the distortion of the site to accommodate either K or Bi gives rise to the proper coordination geometry to yield Raman-active modes. This region would be much weaker in the compounds that do not experience modulation, as supported by the Raman spectra of compounds **I** and **III** (Figure 10). Given that the intensity ratios of these peaks are dependent on the composition of the sample, it is unlikely that the higher-energy peaks are overtones of those at lower energy.

Solid-State NMR. NMR spectroscopy has been a useful tool in studying modulated compounds, and provides structural information that is complementary to the crystallographic data. The NMR line shapes and spin−lattice relaxation times of modulated compounds are known to be strongly dependent on the nature of the modulation vector **q**.[58] The spectral line widths of modulated compounds tend to be broader than those of related compounds without modulation because the loss of translational periodicity gives rise to an essentially infinite number of different chemical

(58) Blinc, R. *Phys. Rep.* (Review Section of Physics Letters) **1981**, *79*, 331−398.

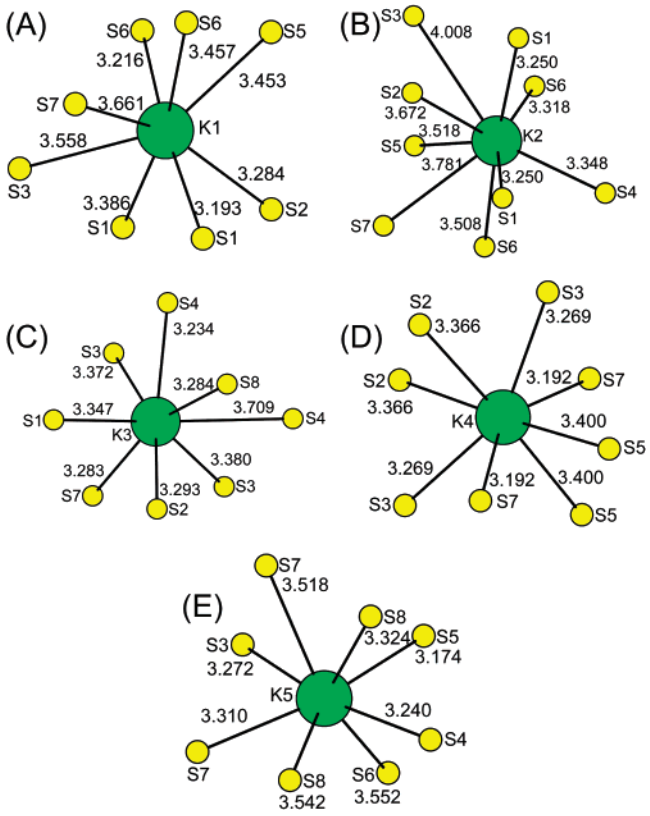

Figure 9. Coordination environment of (A) K(1), (B) K(2), (C) K(3), (D) K(4), and (E) K(5) ions in $K_9Bi(PS_4)_4$.

environments. Therefore, the shielding parameter has a wide range of values, and the spectral line is broadened. Because of enhanced phonon scattering processes, spin−lattice relaxation in incommensurately modulated compounds is more efficient and longitudinal relaxation times tend to be shorter in such compounds.[58]

A summary of the chemical shifts, peak widths, intensities, and T_1 relaxation times for compounds **II** and **III** is found in Table 6, and the spectra of **II** and **III** are displayed in Figure 11. The NMR spectra of **II** indicated two isotropic peaks centered at 88.4 and 71.8 ppm with peak widths of 1150 and 890 Hz, respectively, and a longitudinal relaxation time T_1 of 600(100) s. It is expected that compounds with significant contributions from incommensurate structural modulations have NMR line widths that are broadened and longitudinal relaxation times that are shortened relative to phases that are not modulated.[58] The NMR data on compound **II** indicated only a slight increase in line width but no significant decrease in the longitudinal relaxation time relative to the isoelemental compound **III**. This is consistent with the crystallographic evidence that suggests the effect of the modulation on compound **II** is relatively small.

For compound **II**, the upfield peak at 71.8 ppm had roughly double the integrated intensity of the downfield peak at 88.4 ppm. The crystallographic analysis suggested three unique P atoms, and the NMR intensity data could be explained by an overlap of the peaks arising from two of the P atoms. P(1b) and P(1c) are located within the double chain and have six metal ion neighbors two bonds away. P(1a) bridges neighboring double chains and has five metal

Table 5. Selected Bond Lengths (Å) and Angles (deg) for **III**, with Standard Uncertainties in Parentheses[a]

Bi−S5^{i}	2.842(3)	S5^{i}−Bi−S5	89.05(11)	S8^{i}−K3−S3^{v}	126.85(10)
Bi−S5	2.842(3)	S5^{i}−Bi−S8	93.86(8)	S2^{i}−K3−S3^{v}	158.60(11)
Bi−S8	2.866(4)	S5−Bi−S8	69.38(8)	S1^{xi}−K3−S3^{v}	98.69(9)
Bi−S8^{i}	2.866(4)	S5^{i}−Bi−S8^{i}	69.38(8)	S4^{v}−K3−S3	118.13(11)
Bi−S2	2.877(3)	S5−Bi−S8^{i}	93.86(8)	S7^{x}−K3−S3	64.73(8)
Bi−S2^{i}	2.877(3)	S8−Bi−S8^{i}	156.95(12)	S8^{i}−K3−S3	109.25(11)
		S5^{i}−Bi−S2	175.95(8)	S2^{i}−K3−S3	94.43(8)
K1−S1^{ii}	3.194(5)	S5−Bi−S2	94.04(7)	S1^{xi}−K3−S3	146.18(12)
K1−S6^{ii}	3.215(4)	S8−Bi−S2	84.79(9)	S3^{v}−K3−S3	88.21(9)
K1−S2^{ii}	3.284(3)	S8^{i}−Bi−S2	112.95(9)	S4^{v}−K3−S4	83.0(1)
K1−S1	3.386(5)	S5^{i}−Bi−S2^{i}	94.04(7)	S7^{x}−K3−S4	119.86(10)
K1−S5^{ii}	3.453(3)	S5−Bi−S2^{i}	175.95(8)	S8^{i}−K3−S4	56.48(9)
K1−S6^{iii}	3.457(4)	S8−Bi−S2^{i}	112.95(9)	S2^{i}−K3−S4	92.41(9)
K1−S3	3.558(4)	S8^{i}−Bi−S2^{i}	84.79(9)	S1^{xi}−K3−S4	148.34(12)
K1−S7^{iii}	3.661(4)	S2−Bi−S2^{i}	83.0(1)	S3^{v}−K3−S4	106.37(9)
K1−P1^{ii}	3.664(3)	S1^{ii}−K1−S6^{ii}	170.20(11)	S3−K3−S4	55.20(8)
K1−P2^{ii}	3.790(3)	S1^{ii}−K1−S2^{ii}	61.85(8)	S7−K4−S7^{i}	145.23(13)
K2−S1^{vi}	3.250(5)	S6^{ii}−K1−S2^{ii}	108.47(10)	S7−K4−S3^{vi}	122.32(8)
K2−S1^{vii}	3.251(5)	S1^{ii}−K1−S1	85.44(5)	S7^{i}−K4−S3^{vi}	67.03(7)
K2−S6^{viii}	3.317(4)	S6^{ii}−K1−S1	89.34(11)	S7−K4−S3^{xii}	67.03(7)
K2−S4^{vii}	3.348(4)	S2^{ii}−K1−S1	67.51(9)	S7^{i}−K4−S3^{xii}	122.32(8)
K2−S6	3.508(4)	S1^{ii}−K1−S5^{ii}	116.05(11)	S3^{vi}−K4−S3^{xii}	152.05(13)
K2−S5	3.518(3)	S6^{ii}−K1−S5^{ii}	60.25(8)	S7−K4−S2^{vi}	89.39(8)
K2−S2^{vi}	3.673(3)	S2^{ii}−K1−S5^{ii}	76.74(7)	S7^{i}−K4−S2^{vi}	120.21(9)
K2−P2	3.680(3)	S1−K1−S5^{ii}	121.91(10)	S3^{vi}−K4−S2^{vi}	60.83(8)
K2−P1^{vi}	3.769(3)	S1^{ii}−K1−S6^{iii}	100.37(11)	S3^{xii}−K4−S2^{vi}	95.12(9)
K2−S7	3.781(4)	S6^{ii}−K1−S6^{iii}	85.94(5)	S7−K4−S2^{xii}	120.21(9)
K3−S4^{v}	3.234(4)	S2^{ii}−K1−S6^{iii}	121.83(11)	S7^{i}−K4−S2^{xii}	89.39(8)
K3−S7^{x}	3.283(4)	S1−K1−S6^{iii}	170.52(11)	S3^{vi}−K4−S2^{xii}	95.12(9)
K3−S8^{i}	3.284(4)	S5^{ii}−K1−S6^{iii}	62.30(7)	S3^{xii}−K4−S2^{xii}	60.83(8)
K3−S2^{i}	3.292(4)	S1^{ii}−K1−S3	97.90(9)	S2^{vi}−K4−S2^{xii}	68.98(10)
K3−S1^{xi}	3.347(4)	S6^{ii}−K1−S3	86.14(9)	S7−K4−S5	61.75(7)
K3−S3^{v}	3.372(4)	S2^{ii}−K1−S3	122.53(9)	S7^{i}−K4−S5	89.39(9)
K3−S3	3.380(4)	S1−K1−S3	57.13(8)	S3^{vi}−K4−S5	82.21(7)
K3−S4	3.710(4)	S5^{ii}−K1−S3	146.04(10)	S3^{xii}−K4−S5	121.80(8)
K4−S7	3.192(3)	S6^{iii}−K1−S3	114.24(9)	S2^{vi}−K4−S5	109.67(6)
K4−S7^{i}	3.192(3)	S1^{ii}−K1−S7^{iii}	81.91(9)	S2^{xii}−K4−S5	177.32(8)
K4−S3^{vi}	3.268(3)	S6^{ii}−K1−S7^{iii}	107.89(9)	S7−K4−S5^{i}	89.38(9)
K4−S3^{xii}	3.268(3)	S2^{ii}−K1−S7^{iii}	143.06(11)	S7^{i}−K4−S5^{i}	61.74(7)
K4−S2^{vi}	3.366(3)	S1−K1−S7^{iii}	119.28(9)	S3^{vi}−K4−S5^{i}	121.80(8)
K4−S2^{xii}	3.366(3)	S5^{ii}−K1−S7^{iii}	116.94(8)	S3^{xii}−K4−S5^{i}	82.21(7)
K4−S5	3.400(3)	S6^{iii}−K1−S7^{iii}	54.93(7)	S2^{vi}−K4−S5^{i}	177.32(8)
K4−S5^{i}	3.400(3)	S3−K1−S7^{iii}	66.31(8)	S2^{xii}−K4−S5^{i}	109.67(6)
K5−S5	3.174(4)	S1^{vi}−K2−S1^{vii}	86.79(5)	S5−K4−S5^{i}	71.78(10)
K5−S4	3.239(4)	S1^{vi}−K2−S6^{viii}	89.96(11)	S5−K5−S4	79.56(10)
K5−S3^{vi}	3.272(4)	S1^{vii}−K2−S6^{viii}	159.63(11)	S5−K5−S3^{vi}	85.70(9)
K5−S7^{xiii}	3.310(4)	S1^{vi}−K2−S4^{vii}	93.14(10)	S4−K5−S3^{vi}	165.05(12)
K5−S8^{i}	3.324(4)	S1^{vii}−K2−S4^{vii}	60.90(8)	S5−K5−S7^{xiii}	158.79(11)
K5−S7^{i}	3.518(4)	S6^{viii}−K2−S4^{vii}	99.27(10)	S4−K5−S7^{xiii}	120.65(11)
K5−S8^{xiii}	3.542(4)	S1^{vi}−K2−S6	172.88(13)	S3^{vi}−K5−S7^{xiii}	73.73(8)
K5−S6^{viii}	3.552(4)	S1^{vii}−K2−S6	98.21(11)	S5−K5−S8^{i}	79.79(10)
K5−P2^{xiii}	3.805(4)	S6^{viii}−K2−S6	83.60(5)	S4−K5−S8^{i}	60.97(10)
		S4^{vii}−K2−S6	84.94(9)	S3^{vi}−K5−S8^{i}	118.98(11)
P1−S1	2.020(4)	S1^{vi}−K2−S5	122.35(11)	S7^{xiii}−K5−S8^{i}	114.51(11)
P1−S2	2.080(4)	S1^{vii}−K2−S5	134.49(11)	S5−K5−S7^{i}	87.60(9)
P1−S3	2.032(4)	S6^{viii}−K2−S5	62.98(8)	S4−K5−S7^{i}	118.15(11)
P1−S4	2.018(4)	S4^{vii}−K2−S5	138.2(1)	S3^{vi}−K5−S7^{i}	63.27(8)
P2−S5	2.068(4)	S6−K2−S5	57.01(7)	S7^{xiii}−K5−S7^{i}	87.73(9)
P2−S6	2.007(4)	S1^{vi}−K2−S2^{vi}	57.11(9)	S8^{i}−K5−S7^{i}	57.23(8)
P2−S7	2.023(4)	S1^{vii}−K2−S2^{vi}	64.41(9)	S5−K5−S8^{xiii}	143.94(10)
P2−S8	2.054(4)	S6^{viii}−K2−S2^{vi}	129.10(11)	S4−K5−S8^{xiii}	64.71(9)
		S4^{vii}−K2−S2^{vi}	118.29(8)	S3^{vi}−K5−S8^{xiii}	130.18
		S6−K2−S2^{vi}	129.70(11)	S7^{xiii}−K5−S8^{xiii}	57.10(8)
		S5−K2−S2^{vi}	100.55(8)	S8^{i}−K5−S8^{xiii}	78.8(1)
		S1^{vi}−K2−S7	132.95(11)	S7^{i}−K5−S8^{xiii}	104.44(10)
		S1^{vii}−K2−S7	79.33(9)	S5−K5−S6^{viii}	63.90(8)
		S6^{viii}−K2−S7	116.76(9)	S4−K5−S6^{viii}	85.86(10)
		S4^{vii}−K2−S7	117.35(10)	S3^{vi}−K5−S6^{viii}	85.38(10)
		S6−K2−S7	53.47(8)	S7^{xiii}−K5−S6^{viii}	108.34(10)
		S5−K2−S7	55.16(7)	S8^{i}−K5−S6^{viii}	134.95(11)
		S2^{vi}−K2−S7	76.48(8)	S7^{i}−K5−S6^{viii}	139.56(10)
		P2−K2−S7	31.43(6)	S8^{xiii}−K5−S6^{viii}	115.53(10)
		P1^{vi}−K2−S7	101.97(8)	S4−P1−S1	111.9(2) (10)
		S4^{v}−K3−S7^{x}	131.94(10)	S4−P1−S3	109.04(16)
		S4^{v}−K3−S8^{i}	67.85(9)	S1−P1−S3	110.24(19)
		S7^{x}−K3−S8^{i}	160.19(11)	S4−P1−S2	107.42(16)

Table 5 (Continued)

$S4^{v}-K3-S2^{i}$	134.64(11)	S1−P1−S2	108.60(16)
$S7^{x}-K3-S2^{i}$	89.14(9)	S3−P1−S2	109.56(15)
$S8^{i}-K3-S2^{i}$	72.14(9)	S6−P2−S7	109.34(17)
$S4^{v}-K3-S1^{xi}$	93.46(11)	S6−P2−S8	113.76(18)
$S7^{x}-K3-S1^{xi}$	85.65(12)	S7−P2−S8	107.16(17)
$S8^{i}-K3-S1^{xi}$	92.98(12)	S6−P2−S5	110.70(16)
$S2^{i}-K3-S1^{xi}$	67.88(8)	S7−P2−S5	111.75(16)
$S4^{v}-K3-S3^{v}$	59.84(8)	S8−P2−S5	104.03(17)
$S7^{x}-K3-S3^{v}$	72.78(8)		

[a] Symmetry codes: (i) $-x, -y, z$; (ii) $0.5-x, -0.5+y, -z$; (iii) $x, -1+y, 1+z$; (iv) $x, y, 1+z$; (v) $-x, -1-y, z$; (vi) $x, y, -1+z$; (vii) $0.5-x, 0.5+y, 1-z$; (viii) $0.5-x, -0.5+y, 1-z$; (ix) $x, 1+y, -1+z$; (x) $-x, -y, 1+z$; (xi) $-0.5+x, -0.5-y, 2-z$; (xii) $-x, -y, -1+z$; (xiii) $x, -1+y, z$; (xiv) $0.5-x, 0.5+y, 2-z$; (xv) $0.5+x, -0.5-y, 2-z$; (xvi) $x, 1+y, z$.

Scheme 1

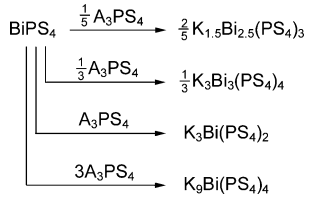

ion neighbors two bonds away. The upfield peak can be attributed to P(1b) and P(1c), which are related by symmetry, and the downfield peak can be attributed to P(1a).

The NMR spectrum of **III** contained two isotropic peaks centered at 86.1 and 79.7 ppm, with 2:5 ratio of signal intensity, line widths of 300 and 640 Hz, and longitudinal relaxation times of 1350 ± 125 and 640 ± 120 s, respectively. There were two crystallographically inequivalent P sites in **III** that could have been assigned to the two peaks observed in the NMR. However, deviations from a 1:1 intensity ratio and different line widths and relaxation times for the two peaks do not support this assignment. A more plausible explanation is that the 64.3 ppm line is due to an impurity that may have been formed by the partial decomposition of compound **III** by moisture. The narrower line

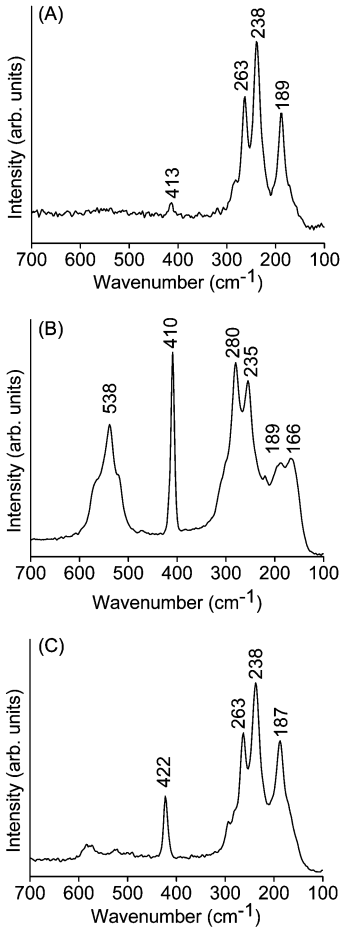

Figure 10. Raman spectra of (A) **I**, (B) **II**, and (C) **III**. The $K_3Bi_3(PS_4)_4$ sample used to collect the spectrum also contained several crystalline impurities (see text).

Table 6. ^{31}P Chemical Shift (CS), Chemical Shift Anisotropy (CSA), and T_1 Values.

compound	CS[a] (ppm)	peak widths (Hz)[a]	integrated intensities[b]	T_1[c] (s)
$K_{1.5}Bi_{2.5}(PS_4)_3$ (**II**)	88.4, 71.8	1150, 890	45.5, 100.0	690(30), 510(60)
$K_9Bi(PS_4)_4$ (**III**)	79.7	640	100	640(120)

[a] Uncertainties in CS are approximately ± 0.5 ppm, and uncertainties in line widths are approximately ± 10 Hz. The chemical shift was determined by a mathematical deconvolution of the peaks after fitting with a Lorentzian line shape, and peak widths were determined by calculating the full width at half-maximum. [b] Intensities were normalized with the most intense peak set to 100. [c] Uncertainties are indicated in parentheses.

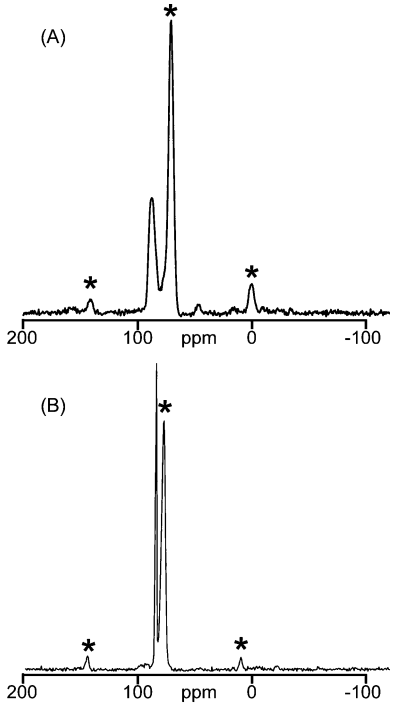

Figure 11. ^{31}P NMR spectra of (A) $K_{1.5}Bi_{2.5}(PS_4)_3$ and (B) $K_9Bi(PS_4)_4$ with isotropic peaks and their spinning sidebands grouped under like symbols.

width is consistent with a new mobile species formed by a reaction of **III** with atmospheric water. Signals from the two crystallographically inequivalent P sites in compound **III** were not resolved and were instead overlapped.

The presence of impurity phases in batches of compound **I** was evident in the X-ray powder diffraction diagrams. These phases are thiophosphate species, as indicated by the large number of peaks in the ^{31}P NMR spectrum. These peaks were not assigned.

Concluding Remarks

It is evident from this work that the group 15 alkali chalcophosphate class of compounds contains a rich and diverse collection of species with wide variability in bonding motifs.[19−25] The present report adds three new compounds to this class, including an example of a phase with an incommensurate structural modulation. Decreased framework dimensionality is favored in compounds with a larger proportion of K_3PS_4. It is interesting to note that there are only several isomorphic compounds in common between the K/Bi/P/S class and the previously reported Tl/Bi/P/S class, namely, $MBiP_2S_7$, and $M_3Bi(PS_4)_2$ (M = K, Tl). None of the new compounds described here have a known Tl^+ analogue, and even though the $K_3Bi_3(PS_4)_4$ and $Tl_3Bi_3(PS_4)_4$ compounds have the same stoichiometry, the structures are quite different.[33] Attempts to form mixed K/Tl solid solutions containing K/Tl/Bi/P/S may produce novel pseudo-quaternary materials with different structures. Finally, flexibility in the Bi coordination in this system is notable, as well as the chemical conditions required to stabilize each compound. The flux conditions previously studied[30] did not identify the title compounds. Thus, the diversity in the group 15 alkali-metal chalcophosphates is even greater than was previously considered and now even includes an example of a modulated compound.

Acknowledgment. Financial support from the National Science Foundation (DMR-0702911) is gratefully acknowledged. We thank Tellurex Corp. for providing us with a gift of bismuth and Hanna Lind for help with the structure of $K_{1.5}Bi_{2.5}(PS_4)_3$.

Supporting Information Available: Tables of atomic coordinates and crystallographic information (CIF). This material is available free of charge via the Internet at http://pubs.acs.org.

IC701211A